materials

MDPI

Article

Characteristics of the Properties of Absodan Plus Sorbent and Its Ability to Remove Phosphates and Chromates from Aqueous Solutions

Eleonora Sočo [1], Andżelika Domoń [2,*], Dorota Papciak [2], Magdalena M. Michel [3], Bogumił Cieniek [4] and Dariusz Pająk [5]

1 Department of Inorganic and Analytical Chemistry, Faculty of Chemistry, Rzeszow University of Technology, 35-959 Rzeszow, Poland; eleonora@prz.edu.pl
2 Department of Water Purification and Protection, Faculty of Civil, Environmental Engineering and Architecture, Rzeszow University of Technology, 35-959 Rzeszow, Poland; dpapciak@prz.edu.pl
3 Institute of Environmental Engineering, Warsaw University of Life Sciences-SGGW, 02-787 Warsaw, Poland; magdalena_michel@sggw.edu.pl
4 Institute of Materials Engineering, College of Natural Sciences, University of Rzeszow, Pigonia 1, 35-310 Rzeszow, Poland; bcieniek@ur.edu.pl
5 Department of Casting and Welding, Faculty of Mechanical Engineering and Aeronautics, Rzeszow University of Technology, 35-959 Rzeszow, Poland; pajak@prz.edu.pl
* Correspondence: adomon@prz.edu.pl

Abstract: The aim of the research was to characterize the parameters of the diatomite sorbent Absodan Plus as well as to assess its suitability for the adsorption of chromates and phosphates from acidic aqueous solutions simulating the conditions occurring in some types of industrial wastewater. The scope of the research includes XRD, SEM, BET, and PZC analyses, and 3D observation of commercial diatomite granules and batch tests to determine the constants of kinetics and the equilibrium of chromates and phosphates adsorption. Absodan Plus is a diatomite commercial material containing an amorphous phase (33%) and is also the crystalline phase of quartz, hematite, and grossite. The material is macro- and mesoporous and its specific surface area is about 30 m^2/g. Its PZC is around pH = 5.5–6.0 and in an acidic environment is able to adsorb the anions. The saturation of the adsorbent surface with molecules of the adsorbed substance occurs after 2 h for chromates and 2.5 h for phosphates. The maximum adsorption capacity of Absodan Plus in terms of phosphorus and chromium amounts to 9.46 mg P/g and 39.1 mg Cr/g, respectively. As shown by XRD analysis, Absodan Plus contains an admixture of hematite, which can support the removal of chromium and phosphorus.

Keywords: chromates and phosphates removal; diatomite; isotherms; kinetics

check for updates

Citation: Sočo, E.; Domoń, A.; Papciak, D.; Michel, M.M.; Cieniek, B.; Pająk, D. Characteristics of the Properties of Absodan Plus Sorbent and Its Ability to Remove Phosphates and Chromates from Aqueous Solutions. *Materials* **2022**, *15*, 3540. https://doi.org/10.3390/ma15103540

Academic Editor: Irene Bavasso

Received: 11 April 2022
Accepted: 13 May 2022
Published: 15 May 2022

Publisher's Note: MDPI stays neutral with regard to jurisdictional claims in published maps and institutional affiliations.

Copyright: © 2022 by the authors. Licensee MDPI, Basel, Switzerland. This article is an open access article distributed under the terms and conditions of the Creative Commons Attribution (CC BY) license (https://creativecommons.org/licenses/by/4.0/).

1. Introduction

Chromium naturally occurs in the environment (air, water, rocks) and contamination of groundwater and soil with chromates can be of natural origin [1], though anthropogenic pollution is the main problem due to the toxicity and genotoxicity of the chromates [2]. The main emitter of chromium water pollution is the energy sector followed by waste and wastewater management, in EU > 80% and about 10% of total emission respectively [3]. In the energy sector, both thermal power plants and refineries generate chromate releases. As has been shown, the leaching of ashes deposited in the lignite power plant is a hexavalent chromium source and results in high contamination of groundwater (even up to 0.120 ppm) [1]. Industrial wastewater has very diverse characteristics. Electroplating wastewater is very rich in hexavalent chrome (400–2000 ppm) and is strongly acidic (pH 2) [4,5]. The tanning industry also generates chromium-rich wastewater. The production is multistage, and the averaged wastewater has a neutral pH and contains up to several

dozen ppm, however, at the pickling and chrome tanning step the acidic wastewater can contain even 2000–3800 ppm of chromium [6,7]. Tannery wastewater can also be slightly alkaline (pH 8) and contain smaller amounts of chromium (several ppm) [8]. Another example of a chromate-contaminated environment is an area of Hanford Site in Washington Stated (USA) [9]. In the production of plutonium in nuclear reactors, a significant amount of chromate has been used as a corrosion inhibitor in reactor cooling water. The deposited chromate sediments and wastes were leached into groundwater and therefore pose an important threat to the environment. Chromite deposits can be the natural source of chromates, as well as anthropogenic, when mining and processing are applied [3]. Especially the poorly managed waste from chromite ore processing is a dangerous factor for the environment [10].

Orthophosphates are a common nontoxic component of the environment. They are desirable for their positive effect on plant cultivation, but their transmission to the aquatic environment has an adverse eutrophication effect [11]. Important point sources of phosphorus pollution are discharges of industrial, municipal, and animal farm wastewater meanwhile, nonpoint pollution is generated by surface runoff from agriculture and urban areas [12,13]. Phosphorus removal from municipal wastewater is efficient at large treatment plants when smaller objects grapple with the lack of effective technology [14]. Even in developed areas of the world, there are still places with no sewage system, from which only partially treated wastewater with nutrients is discharged into the ground [15]. Phosphate rock mining also affects the aquatic environment through runoff of phosphorus-rich drainage waters [16] and phosphate industry processing of raw materials [17]. Industrial wastewater generated in the wet process of phosphoric acid production is characterized by phosphates concentration up to 100 ppm and low pH 2–3 [18,19].

Considering physicochemical techniques, precipitation is used to remove phosphates and chromates from water and wastewater [20] however, it must be noted that during precipitation chromates are additionally reduced to trivalent chromium hydroxide. The wastewater from phosphoric acid production can be treated by precipitation phosphates with ferric and calcium cations even in acidic conditions (pH 3) [18]. Phosphates precipitation connected with ferrous to ferric cation oxidation was also useful to treat wastewater from electroplating in a wide range of pH [21]. Adjustment of pH of neutral pH tannery wastewater to slightly alkaline conditions (pH 8.6–10.3) using NaOH, $Ca(OH)_2$, or MgO allows for a very high precipitation efficiency, close to 100% [22]. The same effect was obtained by adjusting acidic tannery effluent to neutral pH using NaOH [23]. Chromates from tannery effluent also can be very effectively coprecipitated with mixed Fe(II) and Fe(III) cations at slightly acidic to neutral conditions (pH 5–7) [8]. However, precipitation technologies can only be beneficial when the resulting sediments are intermediates for further use, even more so when it requires the use of a large dose of reagents in the case of wastewater with extreme pH and high salinity.

Electrocoagulation is a useful method for phosphates removal from acid manufacturing wastewater [19] and chromates removal from tannery wastewater [7] and synthetic wastewater [24] using aluminum and iron electrodes respectively. The ion exchange technique on strongly basic anion resins is one of many chromate removal methods, although due to the sensitivity of the ion exchangers it is used in drinking water treatment [25]. Metal oxides, especially iron oxide, are characterized by the ability to adsorb chromates and phosphates. Iron and manganese oxides, being residues from groundwater treatment, has been evaluated as good adsorbent for chromates removal [26]. The iron precipitates of biogenic origin are also positively assessed for the removal of this pollutant [5]. Iron oxides are often used as coatings on mineral carriers and in this form, they adsorb phosphates [27,28]. The common feature is that the adsorption of chromates and phosphates is intensified under acidic conditions due to electrostatic attraction, ion exchange, and complexation with protonated surfaces [12]. Mineral materials such as indigenous volcanic rock [29], aluminosilicate rock containing feldspar, montmorillonite, and illite [30], diatomite, and

zeolite [31], dolomite and opoka [32], zeolitic tuff [33] are also used to remove chromates and phosphates.

Diatomite is a siliceous sedimentary rock with a predominant opal content and a smaller amount of quartz, calcite, clay minerals, iron compounds, or glauconite [34]. Its biogenic nature comes from the shells of diatoms that build diatomite and give the rock a porous structure. The lithological variability between deposits and even within one deposit results in differentiated porosity, density, specific surface area, and adsorption capacity of diatomite [35–37]. As a result, diatomite sorbents may have different properties depending on their origin. Meso- and macroporosity is a characteristic feature of this material, due to which it is widely used as a filtration aid in many industrial and environmental applications and the porosity can be additionally increased by heat processing [38,39] or acid treatment [40]. Diatomite is used in various industrial applications as a filler, carrier, holder, sorbent, abrasive, and ingredient [35].

The known use of diatomite is the production of diatomaceous sorbents for the removal of oil spills and other petroleum contaminants [41,42]. Diatomite can also be used as a filling in biosorption filters as it stimulates the growth of the nitrifying biofilm [42,43]. Diatomite has the ability to adsorption of cations by ion exchange and electrostatic attraction with dissociated silanol groups [44]. In this way, the raw diatomite can remove Pb, Cu, Cd, Ni, and Ag cations from water solutions [39,45,46]. In an acidic environment, the surface of diatomite undergoes protonation and as a result, it is able to adsorb oxyanions like chromate, phosphate, and arsenite [32,47–50]. This proves the possible use of diatomite in the treatment of wastewater containing chromates and phosphates. Other studies show that opal-A is of little importance for the adsorption of arsenates, but there is a correlation between the effectiveness of their removal and the content of iron oxide being the natural impurities of the rock [51]. This is an important premise, indicating that the parent rock admixtures have a significant impact on their adsorption properties, therefore particular commercial diatomite sorbents may have different effectiveness. The unique properties of diatomite enable its widespread and multi-sector use. The USA (35%) and China (19%) dominate the world diatomite market, but the EU produces around 13% of the global product [52]. Diatomite sorbents for general purposes are popular in the trade. They are dedicated to the removal of pollutants from the environment as well as to protecting the environment against contamination from entering it. Commercial universal diatomite sorbents are designed to remove liquid substances such as oils, fuels, paints, inks, acids, bases, water coolants, and other solvents from industrial floors [53–55]. Research on the use of diatomite for heavy metal removal is important because it is an abundant, low-cost eco-environmental functional material [38,56]. There are many studies on the sorption on diatomites from various quarries [35,36,39,40,42,48,49,56], but these are not commercial products. The popular diatomite sorbent Absodan Plus (AP) is intended for a wide range of applications [55], however, research was carried out in the field of removing petroleum derivatives oil [57]. Also, it is important to determine the sorption capacity of commercial diatomites for other non-standard applications (not specified by the manufacturer), as these materials are potentially available.

The aim of the research was to characterize the material parameters of the commercial diatomite sorbent Absodan Plus as well as to assess its suitability for the adsorption of chromates and phosphates from acidic aqueous solutions simulating the conditions occurring in some types of industrial wastewater. The scope of the research includes: X-ray diffraction (XRD), scanning electron microscopy (SEM) analysis, Brunauer-Emmett-Teller (BET) surface area analysis, point of zero charge (PZC) analysis, and 3D observation of commercial Absodan Plus granules as well as batch tests to determine constants of kinetics and equilibrium of chromates and phosphates adsorption.

2. Materials and Methods

2.1. Adsorbent

2.1.1. Characteristics of Absodan Plus

The diatomite sorbent Absodan Plus (Damolin, Katowice, Poland) was used for the tests, which, according to the safety data sheet, is calcined diatomaceous earth. Its main application is the removal of liquid substances such as fats, greases, oils, fuels, and water from the ground. It is also designed to absorb bases, acids, solvents, and impurities from water solutions. An exception is a hydrofluoric acid due to the large amounts of SiO_2. Absodan Plus is nonflammable, harmless, chemically inert, and odorless. It has many advantages, as it does not release the absorbed liquid, has a high absorption capacity of up to 130% of its weight, and allows multiple uses [55]. The chemical composition of the tested diatomite is presented in Table 1.

Table 1. Physicochemical properties of the tested diatomite—Absodan Plus (safety data sheet) [based on ref. [55]].

Parameter	Value	Parameter	Value
SiO_2, % (*w*/*w*)	75	MgO, % (*w*/*w*)	2
Al_2O_3, % (*w*/*w*)	7	$K_2O + Na_2O$, % (*w*/*w*)	2
Fe_2O_3, % (*w*/*w*)	9	Residue on ignition (1025 °C), % (*w*/*w*)	2
TiO_2, % (*w*/*w*)	1	Weight density, g/mL	2.3
MnO_2, % (*w*/*w*)	1	pH (10% suspended solids)	5.5
CaO, % (*w*/*w*)	1	Bulk density, g/L	509

2.1.2. Analysis of Absodan Plus Properties

A detailed study was conducted to evaluate Absodan Plus's structure, chemical composition, and properties. The samples of diatomite were subjected to the following set of analyses:

- X-ray diffraction analysis (XRD): The mineral composition of diatomite was assessed using X-ray diffraction with $CuK_{\alpha 1}$ radiation, with scan step 0.015 degrees, scan rate 2 s/step, and scan range from 17 to 70° 2θ at 40 kV and 40 mA (Bruker D8 Advance, Bruker AXS, Germany). The average crystallite sizes (D) of samples were calculated from the XRD data by applying the Debye–Scherrer Equation: $D = 0.89\lambda/B\cos\Theta$, where λ is the wavelength of the X-ray in nanometres, B is the peak width at half-height (FWHM), and θ is the angle between the incident and diffracted beams in angular degrees.
- Crystallinity and amorphous % of diatomite from its scan were computed with Bruker Eva software, as follows:

$$\% \text{ Amorphous} = ((\text{Global area} - \text{Reduced area})/\text{Global area}) \times 100$$
$$\% \text{ Crystallinity} = 100 - \% \text{ Amorphous}.$$

- SEM microscopic analysis: The morphological and textural observation of the surface was made by scanning electron microscope (SEM) (TESCAN VEGA 3, Fuveau France). SEM was used also with a back-scattered electron detector (BSE) (INCA x-act, Oxford Instruments) to broaden the scope of the element content analysis.
- Brunauer-Emmett-Teller (BET) surface area analysis: Specific surface area and total pore volume were determined using low-temperature nitrogen adsorption-desorption isotherms using an ASAP 2020 porosimeter (Micromeritics, Norcross, GA, USA). Before measurements, the samples were degassed at 200 °C. The specific surface area and total pore volume were calculated by the Brunauer-Emmett-Teller (BET) method and the Barrett-Joyner-Halenda (BJH) method, respectively.
- Stereoscopic image of the diatomite was analyzed by X2000 series microscopes (Opta-Tech, Warsaw, Poland) are designed for observation of small, 3D objects in transmitted and reflected light, and the 2D surface of diatomite measurements of topography,

and layer thickness were carried out by confocal 3D microscope (NanoFocus, Oberhausen, Germany).

- Fourier transform infrared spectroscopy (FTIR) analysis: FTIR spectra of Absodan Plus were obtained with an Alpha spectrometer (Bruker, Billerica, MA, USA). The tests were carried out with the transmission method, using the technique of pressing samples with potassium bromide. Compressed adsorbent samples were mixed with KBr at a constant adsorbent weight to KBr weight ratio of 0.25% and pelleted under pressure. The FTIR spectra were employed in a spectral range of 4000 to 500 cm^{-1} [58].
- Determination of point of zero charge (PZC) of diatomite: The PZC was determined using three methods:
  1. Suspension method: In a series of 250-mL Erlenmeyer flasks, 0.5 g of diatomite was added to 50.0 mL of 0.1 M $NaNO_3$ solution. The pH was adjusted with 0.1 M HNO_3 and 0.1 M NaOH as needed, to obtain the appropriate pH values of 2, 3, 4, 5, 6, 7, 8, 9, 10, and 11. The samples were shaken for 12 h using a shaker: vibration amplitude 8.5; rate 180 (ELPIN PLUS, type 358 A, Lubawa, Poland). After settling, the pH values of the supernatant in each flask were again measured. After settling, the pH values of the supernatant in each flask were again measured [59,60].
  2. Potentiometric method: Three flasks containing 0.05 g of diatomite, 3 mL of 0.1 M $NaNO_3$ (to establish an ionic strength constant), and 1 mL of 0.01 M NaOH were added to 6 mL of distilled water. Then all samples were titrated with 0.01 M HCl. Based on the obtained data, a plot of the dependence of the potential change [mV] on the volume of titrant consumed [mL] was made. The research was carried out for a blank and a test sample. The diatomite potential was measured using a combination glass electrode (Elmetron, type OSH 10-00, Zabrze, Poland) [59,60].
  3. Hahn'a Method: The method consists in determining the highest increase of the potential ($\Delta E_{\max}$) and two adjacent potential values that lie on both sides of it (ΔE_1, ΔE_2). Based on these values, the correction (x_b) is calculated, which increases the accuracy of the PZC determination (the correction enables the precise determination of the volume of the titrant at the place of its occurrence [61]. The calculations were done according to Equation (1):

$$x_b = \frac{\Delta V \cdot \Delta E_2}{2 \cdot \Delta E_1} \quad (1)$$

where:

x_b—correction,
ΔV—a volume of titrant,
$\Delta E1$—a potential gain that occurs before ΔE_{max}.

2.2. Adsorbate

The sorption of phosphates and chromates on diatomite was studied by batch experiments. The concentration of phosphates and chromates after the sorption process was determined using a UV-VIS spectrophotometer (JASCO, model V-670) at the wavelength λ = 720 nm and two absorption maxima of 350 nm and 373 nm.

- Determination of the concentration of phosphates ions by the molybdenum blue method: The standard curve was prepared based on a series of phosphates ions solutions with concentrations ranging from 0 to 1.7 mg/L. The absorbance of the prepared solutions was measured against the reagent blank (sample without the addition of phosphates ions). Immediately before the measurement, 1.5 mL of ammonium molybdate and 2 drops of tin (II) chloride (reducing agent in the reaction of the formation of navy blue molybdenum blue) were added to each of the samples. Because the molybdenum method cannot determine strongly acidic or basic aqueous solutions, all samples were neutralized by adding six drops of 6 M NaOH each. The standard

curve equation was determined by linear regression using the least-squares method. The determined proper absorption coefficient (ε), corresponding to the slope in the straight line equation, was 0.28 L/mg·cm (Figure 1a).

- Determination of the concentration of chromates ions by the chromate method (UV/VIS spectrophotometry): Absorbance measurements were performed for given standard solutions with known concentrations in the range of 0 to 35 mg/L. The absorbance of the prepared solutions was measured against the blank reagent (a sample without the addition of chromates ions. The determined proper absorption coefficient (ε) was 0.03 L/mg·cm (Figure 1b).

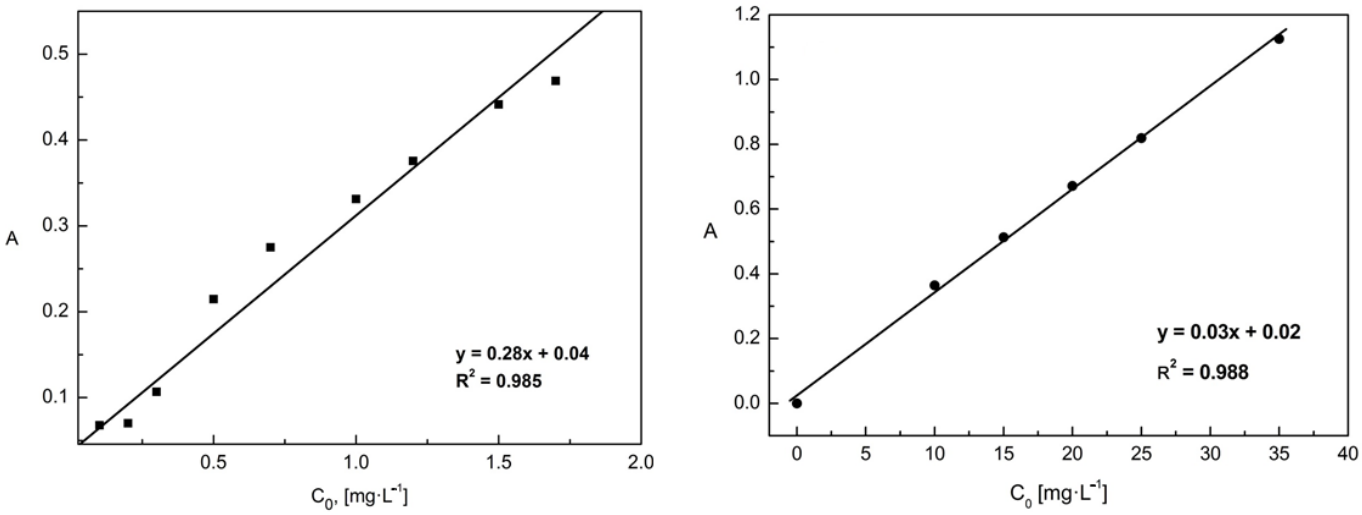

(**a**) (**b**)

Figure 1. Determined appropriate absorption coefficient (ε) necessary for the determination concentration of: (**a**) phosphates ions and (**b**) chromates ions.

2.3. Batch Studies of the Adsorption Process

2.3.1. Effect of Shaking Time on Adsorption

0.5 g of diatomite and 50 mL of a solution of phosphates or chromates ions at a concentration of 50 mg/L were added to 6 flasks with a capacity of 100 mL. The pH of the solutions was adjusted to 2 with 6 M HNO_3 to create conditions typical of acidic industrial wastewater [34,35,48,49]. The prepared samples were shaken for 15–400 min, then the suspension obtained was filtered on a filter paper. The content of phosphates or chromates was determined in the supernatant.

2.3.2. Effect of Adsorbent Concentration on Adsorption

0.5 g of diatomite and 50 mL of previously prepared solutions of phosphates or chromates (pH 2) with concentrations of 10, 50, 200, 350, 400, 1000, 2000, and 3000 mg·L^{-1} were added to 5 flasks with a capacity of 100 mL. Then they were placed on a shaker, and adsorption was carried out for 1.5 h. After this time, the resulting mixture was filtered on a filter paper, and the content of phosphates or chromates was determined in the filtrate.

2.4. Models of Equilibrium and Kinetics of Adsorption

To fully understand the adsorption nature of phosphates or chromates ions in commercial diatomite sorbent, graphs of Freundlich, Langmuir, Halsey, Jovanovich, and Redlich-Peterson isotherms were prepared [Table 2] [62]. On their basis, it was determined which isotherm equation describes the studied phenomenon most accurately. The coefficient of determination (R^2) and the chi-square statistic reduced by the number of degrees of freedom (χ^2/DoF) were used to define the fit of the models to the results of the experiment. The calculations were made in Origin 7.5. The kinetic evaluation of the realized adsorption

process was also performed with the use of pseudo-first and pseudo-second-order kinetic models [Table 3].

To determine the rate-limiting stage of the adsorption process, the intraparticle diffusion model developed by Weber and Morris [63] was used. This model is presented in the Table 3.

Table 2. Lists of adsorption isotherm models.

Isotherms	Equation	Abbreviations	References
Freundlich	$q_e = K_F \cdot (C_e)^{\frac{1}{n}}$	q_e—the equilibrium concentration of the adsorbate on the adsorbent surface [$mg \cdot g^{-1}$], K_F—Freundlich adsorption equilibrium constant [$mg^{1-1/n} \cdot L^{1/n} \cdot g^{-1}$], C_e—the concentration of the adsorbate in the solution at equilibrium [$mg \cdot L^{-1}$], n—adsorption intensity, q_{max}—maximum adsorption capacity [$mg \cdot g^{-1}$], K_L—Langmuir adsorption equilibrium constant [$L \cdot mg^{-1}$], a_R—Redlich-Peterson constant [$L \cdot mg^{-1}]^{\beta R}$, K_R—Redlich-Peterson adsorption equilibrium constant [$L \cdot g^{-1}$], βR—parameter dependent on the concentration of the adsorbate, K_J—Jovanovich adsorption equilibrium constant [$L \cdot g^{-1}$], K_H—Halsey adsorption equilibrium constant [$mg^{n+1} \cdot g^{-1} \cdot L^{-1}$].	[64,65]
Langmuir	$q_e = q_{max} \cdot \frac{K_L \cdot C_e}{1+K_L \cdot C_e}$		[65–67]
Jovanovich	$q_e = q_{max} \cdot \left(1 - e^{(K_J \cdot C_e)}\right)$		[68]
Halsey	$q_e = (K_h \cdot C_e)^{\frac{1}{n}}$		[69,70]
Redlich-Peterson	$q_e = \frac{K_R \cdot C_e}{1+a_R \cdot C_e^{\beta R}}$		[64–67]

Table 3. Lists of kinetic models [71].

Kinetic Model	Pseudo-First-Order (PFO)	Pseudo-Second-Order (PSO)	Intra-Particle Diffusion
Equation	$dq/dt = k_1(q_e - q_t)$ $q_t = q_e(1 - e^{-k_1 t})$	$dq/dt = k_2(q_e - q_t)^2$ $q_t = k_2 q_e^2 t/(1 + k_2 q_e t)$	$q_t = k_i t^{1/2} + b_i$
where: q_t—adsorption capacity (in time t) [$mg \cdot g^{-1}$], k_i—the intra-particle diffusion rate constant for adsorption [$mg \cdot g^{-1} \cdot min^{1/2}$], b_i—the boundary layer thickness [$mg \cdot g^{-1}$].			

3. Results and Discussion

3.1. Adsorbent Characteristics

SEM microscopic observations allowed to characterize the morphology of the diatomite (Figure 2). The surface composed of mesopores and macropores indicates high porosity and low density of this material, which was also observed in previous studies [57]. The results of the BET analysis show that the specific surface area of the Absodan Plus was 30.6 m^2/g, while the total pore volume was 0.46 cm^3/g. The stereoscopic and two-dimensional 2D image of diatomaceous earth together with the layer thickness is shown in Figure 2. XRD analysis of Absodan Plus showed that quartz, hematite, and grossite are the main minerals of the crystalline phase. They were found approximately in the 2.73:1:2.68 ratio, respectively (Figure 3). As a result of the adsorption of chromates and phosphates ions, the structure of the diatomite slightly changes. XRD analysis performed confirms the change in the size of the crystallites and grains of the adsorbent tested (Figure 3). A strong diffraction peak (1 0 1) at 26.60° 2θ comes from quartz (Figure 4). Based on this peak, the crystallite size (D) was calculated for three samples (Table 4). The change in crystallite size is not significant and remains in the same order of magnitude. Crystallinity and amorphous ratio are shown in Table 4. Diatomite adsorbent is characterized by a twice higher proportion of the crystalline phase as compared to the amorphous phase. The presence of phosphate and chromate adsorbates does not significantly affect the proportion of these phases.

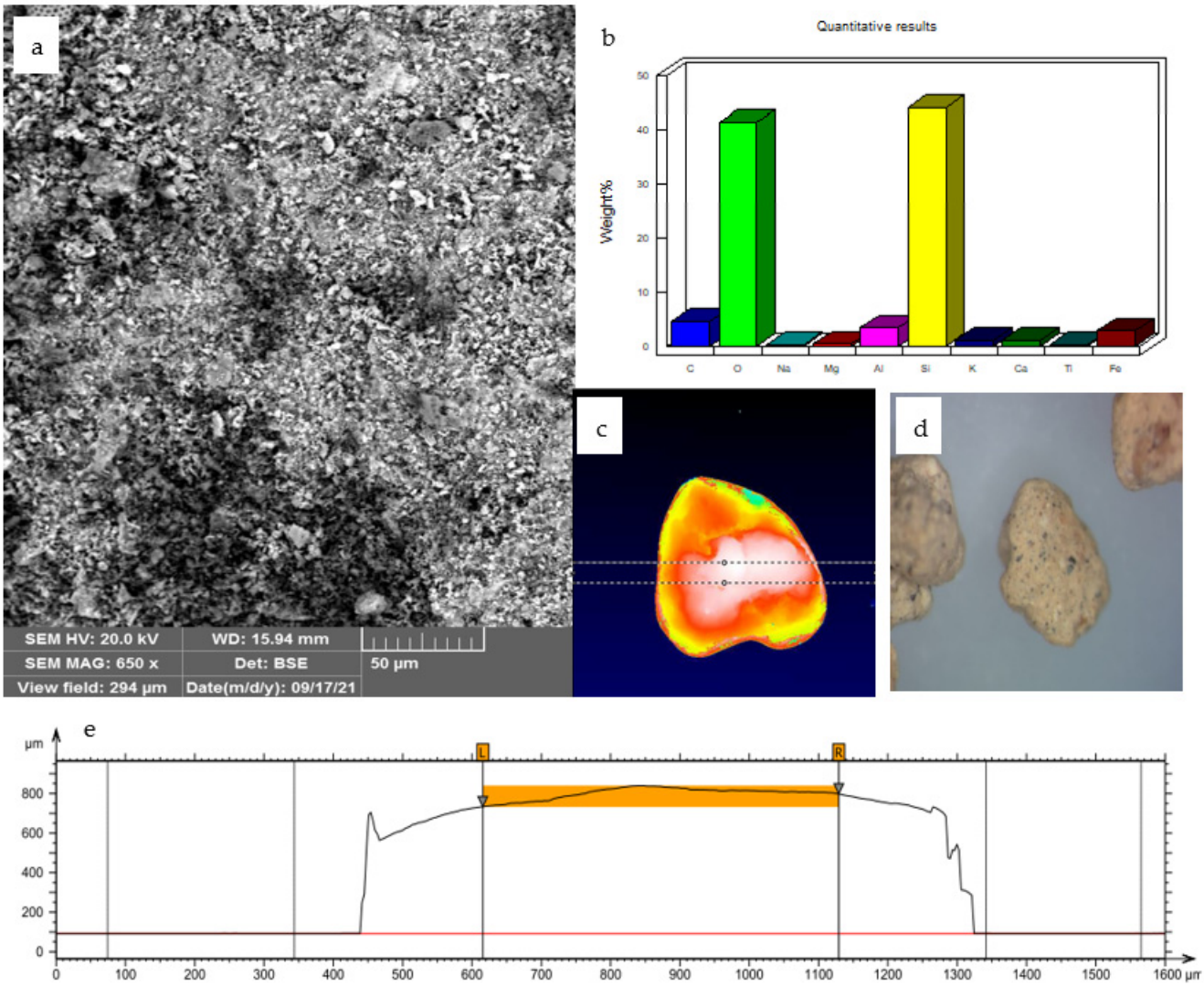

Figure 2. Absodan Plus: (**a**) SEM surface micrograph (650×), (**b**) content of identified elements diatomite, (**c**) 2D image (**d**) stereoscopic image, (**e**) topography layer (extracted profile: maximum height 747 µm, mean height 710 µm).

Table 4. Crystallinity and the amorphous ratio of Absodan Plus take into account the size of crystallites.

Sample	Crystallite Size, Å	Crystallinity, %	Amorphous, %
AP	342	66.6	33.4
AP + chromates ions	552	66.0	34.0
AP + phosphates ions	408	68.6	31.4

The FTIR spectrum was performed to identify functional groups on the surface of the adsorbent used. As a result, it was possible to observe the structural changes caused by the ongoing adsorption process. This is especially important from the point of view of regenerating this type of adsorbent, and thus the possibility of its multiple uses in subsequent processes. The spectrum analysis is shown in Table 5.

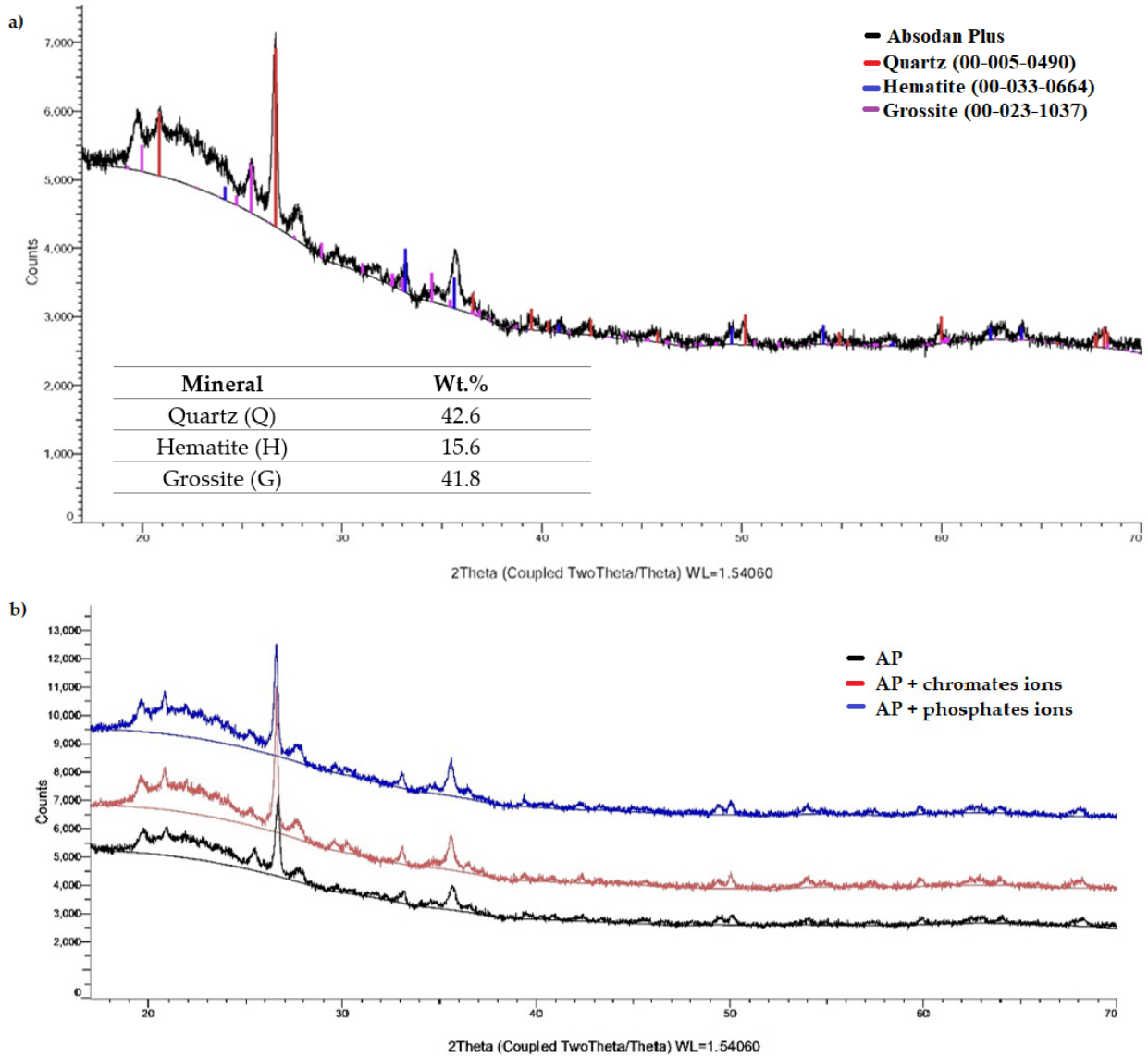

Mineral	Wt.%
Quartz (Q)	42.6
Hematite (H)	15.6
Grossite (G)	41.8

Figure 3. XRD diffractograms of: (**a**) Absodan Plus, (**b**) Absodan Plus with chromates and phosphates ions.

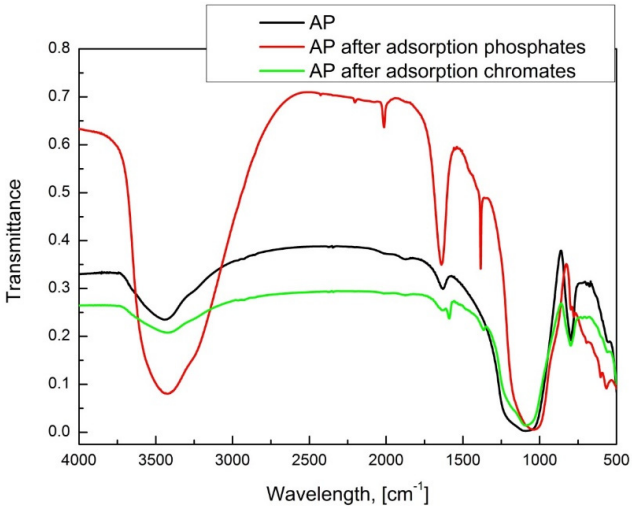

Figure 4. FTIR analysis of Absodan Plus samples.

Table 5. Analysis of the FTIR absorption spectrum of Absodan Plus samples-characteristic bands.

Wavelength, [cm^{-1}]	Band Description	The Band Comes from:
3443	Very wide, high intensity	the stretching vibrations of the –OH group.
1643	Narrow, low intensity	the stretching vibrations of the groups: C=C, CO-CH_2-CO
1386	Very narrow, low intensity	the adsorbed PO_3^{4-} ion
1076	Broad, high intensity	the stretching vibrations of the C-O groups
796	Narrow, low intensity	the stretching vibrations of asymmetric C-H groups; band located in the dactyloscopy area

In all the spectra of the tested samples of Absodan Plus, there are characteristic bands in the following areas: 3440 cm^{-1}, 1630 cm^{-1}, 1050 $cm^{-1,}$ and 800 cm^{-1} (Figure 4). The band around 3443 cm^{-1} can come from both the hydroxyl groups that build the water molecule and those that have been bonded to the AP surface by chemical bonds. The band located at the value of 1643 cm^{-1} indicates the presence of C=C bonds and carboxyl-carbonate structures. The most intense of the bands located at 1076 cm^{-1} comes from vibrations of C-O bonds that occur in ether, carboxyl, and phenol groups. The band at the value of 796 cm^{-1} is the result of the presence of SiO_4^{4-} and AlO_4^{5-} systems in the tetrahedral samples, forming the three-dimensional structure of diatomites [72].

In the spectra of the samples after the adsorption process, an additional band appears at the wavenumber value of 1386 cm^{-1}. It was suspected that it could be derived from an adsorbed orthophosphate (V) ion or a complex formed by it. To verify the thesis, the experimental spectrum was correlated with the FTIR spectrum of sodium dihydrogen phosphate, the source of phosphate ions in the conducted research. It turned out that there is a characteristic band in the range of 1300–1400 cm^{-1}. This fact confirms that the 1386 cm^{-1} band is derived from molecules of the adsorbate attached to the AP surface (Figure 4). After analyzing the spectroscopic spectra, it was found that the process of adsorption of phosphate ions and, to a lesser extent, chromate ions take place.

The value of the zero point of the adsorbent load determined by the suspension method was 5.6 (Figure 5a). PZC is the point of intersection of the plot of the dependence ΔpH = f (pH 0) with the OX axis, therefore it is equivalent to the zero point of this function. In the case of the potentiometric method, the PZC was 5.5 (Figure 5b). The value was read from the graph of the dependence of the potential change [mV] on the volume of used titrant [mL]-PZC is located at the intersection of the lines on the graphs. PZC determined by Hahn's method was 5.9 [Table 6], its average value fluctuates around pH = 5.5–6.0, i.e., in the area classifying the reaction of the environment as slightly acidic. The pH of the aqueous diatomite solution was 5.2, which is below the zero point of the electric charge. This means that the Absodan Plus surface is positively charged, and it has a greater ability to attach anions than cations. Speciation of phosphorus and chromium anions is strongly pH-dependent. The experiment was carried out in an acidic environment (pH 2), and in the range of the concentrations used, the anions were not fully dissociated. Phosphorus was present as H_3PO_4 and $H_2PO_4^-$ with a slight quantitative predominance of the undissociated form [73]. Under these conditions, the dominant form of chromate was partially dissociated $HCrO_4^-$ (~80%) and in a dozen or so percent $Cr_2O_7^{2-}$ [74], as well as the possible content of undissociated acid H_2CrO_4 [75]. This allows the conclusion that the conditions of the experiment are favorable because a positively charged surface would interact with the anions as a result of electrostatic attraction [75].

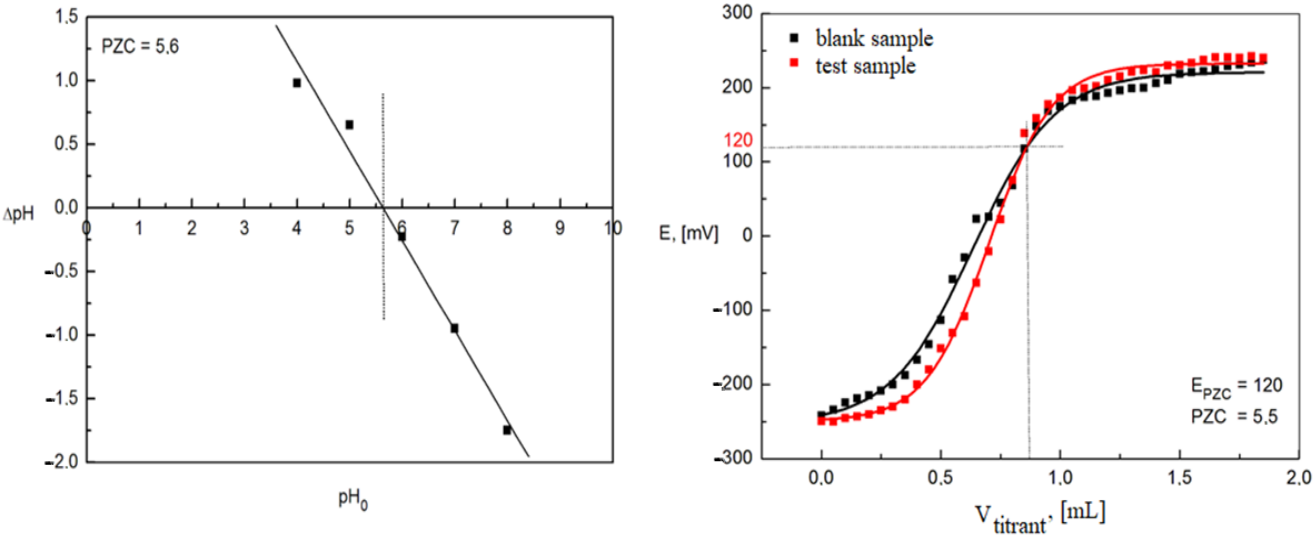

(**a**) (**b**)

Figure 5. PZC of the adsorbent: (**a**) suspension method; (**b**) potentiometric method.

Table 6. Values from the titration table based on which the PZC was determined by Hahn's method.

Parameter	ΔE1	ΔEmax	ΔE2	$pH_{0.8}$ *
Value	63.4 mV	52.8 mV	43.4 mV	5.9

* index 0.8 is the volume of added titrant at the PZC point, [mL].

3.2. The Adsorption Equilibrium

The adsorption isotherms of phosphates ions (Figure 6) and chromates ions (Figure 7) were prepared to select the model that best describes the adsorption process on Absoban Plus. Each of the isotherms is represented by the relation $q_e = f(C_e)$. The following isotherms were made: Halsey, Jovanovich, Langmuir, Redlich-Paterson, and Freundlich. The comparisons of isothermal models for adsorbed phosphates and chromates ions are presented in Figures 6 and 7. The parameters obtained for all isothermal models for adsorbed chromates and phosphates ions are presented in Table 7.

A good fit to the experimental points is represented by those isotherms that determine the relationship $q_e = f(C_e)$. The parameters determined from each of these equations can help assess the adsorption efficiency, the affinity of the adsorbent for the adsorbate, and whether the sorption system used is favorable or not.

The Redlich-Peterson isotherm was the best fit for the experimental points. This is confirmed by the calculated coefficient of determination, which for this model has the highest value: R^2 = 0.975 (chromates ions) and 0.994 (phosphates ions). The error in fitting the theoretical curve to the experimental data also reaches the smallest value (χ^2 = 6.0 and 8.5, respectively) (Table 7). The parameters of this equation are, in the case of chromium ions, respectively: K_{RP} = 29.7 L·g^{-1}, a_{RP} = 1.13 L·mg^{-1} and B = 0.8. For phosphates ions, the parameters assume the following values: K_{RP} = 255 L·g^{-1}, a_{RP} = 40.3 L·mg^{-1} and B = 0.8 (Table 7). The worst fit shows the Halsey isotherm, for which the value of R^2 is <0.1 and the value of χ^2/DoF is 520 (phosphates ions) and 4320 (chromates ions). The Halsey model is used for multilayer adsorption on the heterogeneous surface [76], which does not occur with the adsorption performed.

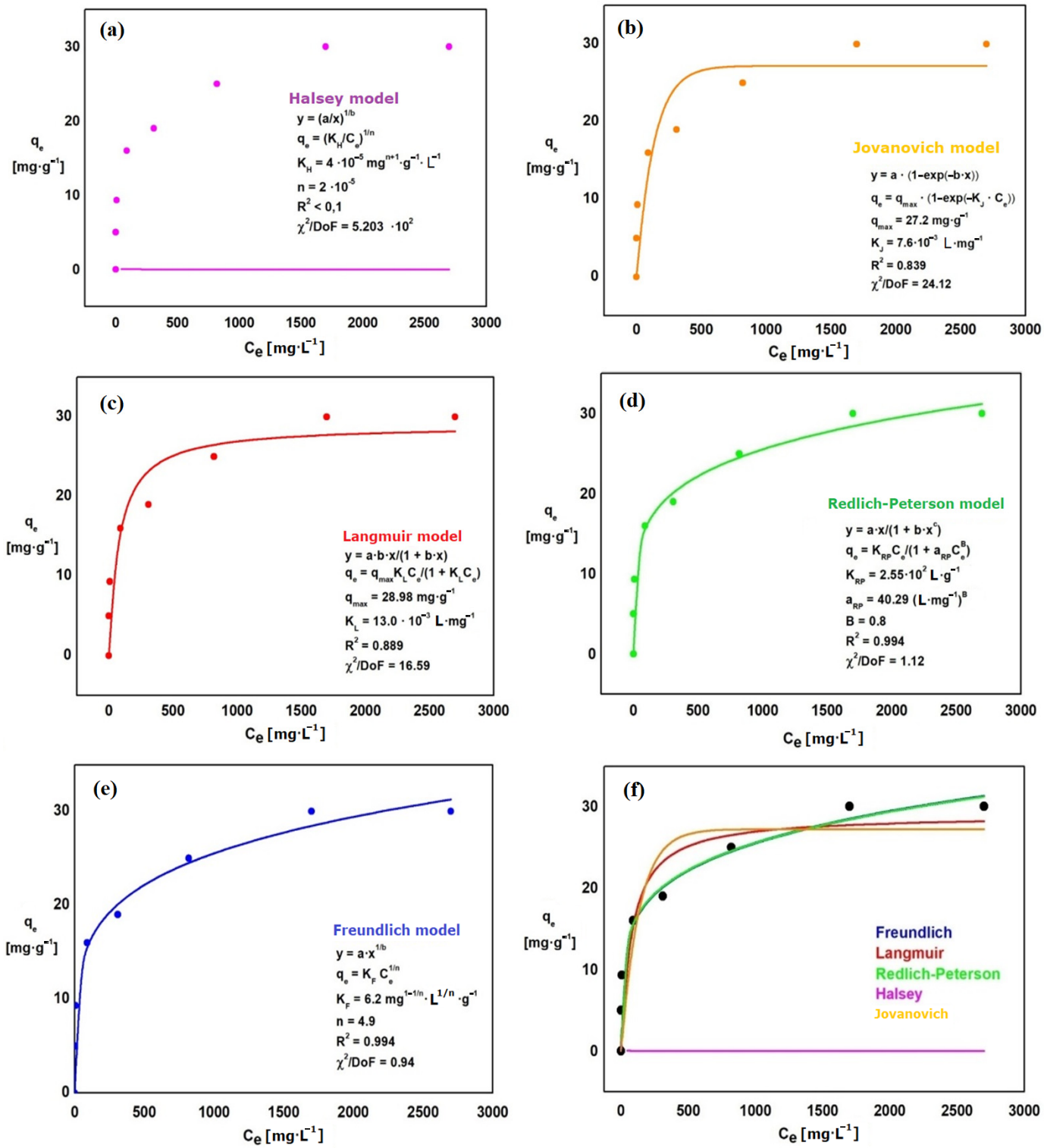

Figure 6. Isotherms: Halsey (**a**), Jovanovich (**b**), Langmuir (**c**), Redlich-Peterson (**d**), Freundlich (**e**), comparison of isothermal models for adsorbed phosphates ions (**f**).

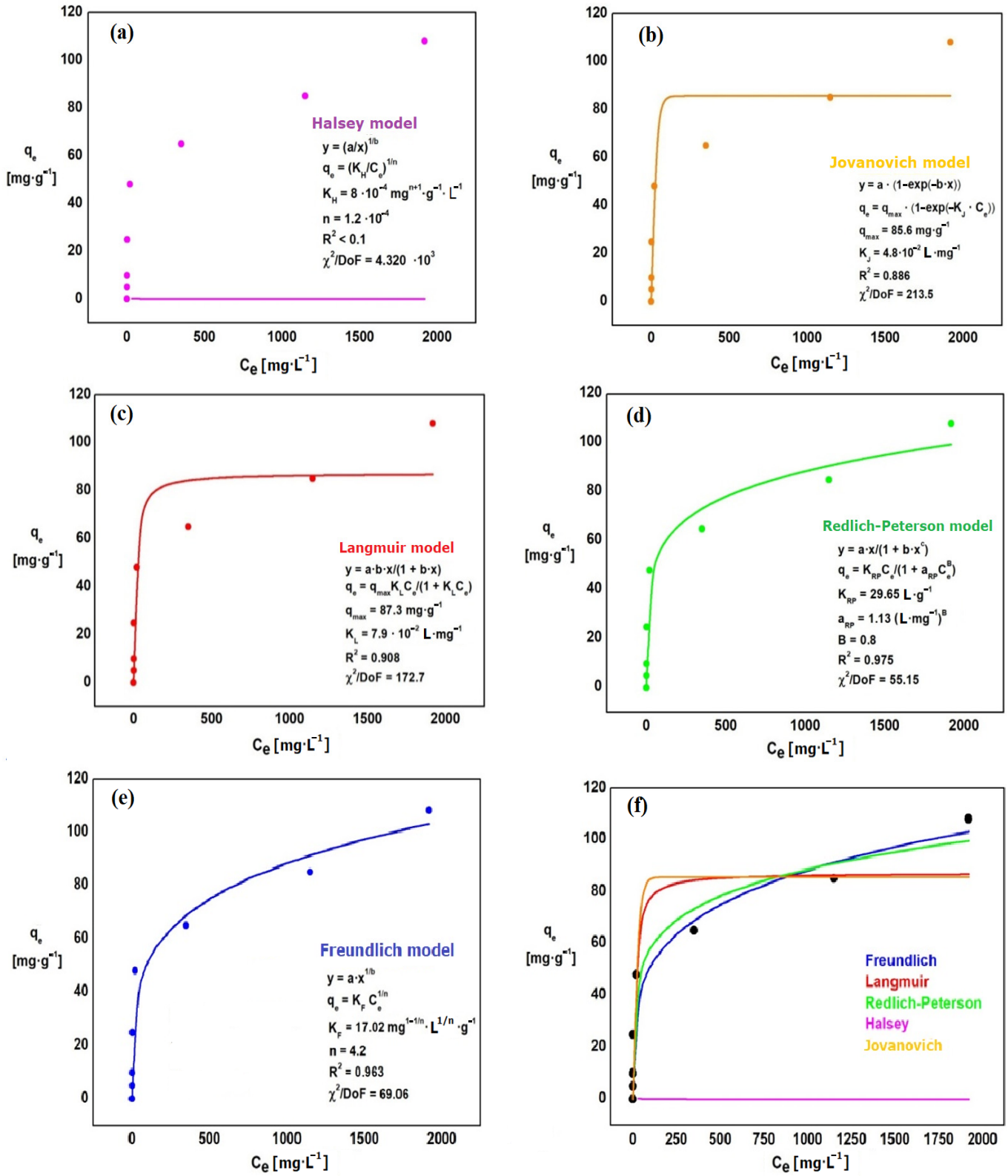

Figure 7. Isotherms: Halsey (**a**), Jovanovich (**b**), Langmuir (**c**), Redlich-Peterson (**d**), Freundlich (**e**), comparison of isothermal models for adsorbed chromates ions (**f**).

Table 7. Isotherm parameters for the adsorbed phosphates and chromates ions.

Phosphates Ions					Chromates Ions				
Halsey isotherm									
K_H [$mg^{n+1} \cdot g^{-1} \cdot L^{-1}$]	n		R^2	X^2/DoF	K_H [$mg^{n+1} \cdot g^{-1} \cdot L^{-1}$]	n		R^2	X^2/DoF
$4 \cdot 10^{-5}$	$2 \cdot 10^{-5}$		<0.1	520	$8 \cdot 10^{-4}$	$1.2 \cdot 10^{-4}$		<0.1	4320
Jovanovich isotherm									
K_J [$L \cdot mg^{-1}$]	q_{max} [$mg \cdot g^{-1}$]		R^2	X^2/DoF	K_J [$L \cdot mg^{-1}$]	q_{max} [$mg \cdot g^{-1}$]		R^2	X^2/DoF
0.008	27.2		0.839	24.1	0.048	85.6		0.886	213
Langmuir isotherm									
K_L [$L \cdot mg^{-1}$]	q_{max} [$mg \cdot g^{-1}$]		R^2	X^2/DoF	K_L [$L \cdot mg^{-1}$]	q_{max} [$mg \cdot g^{-1}$]		R^2	X^2/DoF
0.013	28.9		0.889	16.6	0.079	87.3		0.908	173
Freundlich isotherm									
K_F [$mg^{1-1/n} \cdot L^{1/n} \cdot g^{-1}$]	n		R^2	X^2/DoF	K_F [$mg^{1-1/n} \cdot L^{1/n} \cdot g^{-1}$]	n		R^2	X^2/DoF
6.2	4.9		0.994	0.94	17.0	4.2		0.963	69.1
Redlich-Peterson isotherm									
K_{RP} [$L \cdot g^{-1}$]	a_{RP} [$L \cdot mg^{-1}$]	B	R^2	X^2/DoF	K_{RP} [$L \cdot g^{-1}$]	a_{RP} [$L \cdot mg^{-1}$]	B	R^2	X^2/DoF
255	40.3	0.8	0.994	1.12	29.7	1.13	0.8	0.975	55.2

The $\frac{1}{n}$ parameter in the Freundlich isotherm characterizes the surface of the adsorbent. The values should be between 0 and 1. The closer the value to $\frac{1}{n}$ is to 0, the more ideal the adsorbent surface is. On the other hand, values of $\frac{1}{n}$ close to 1 define the surface as heterogeneous. In the experiment, the value of n was determined at 4.2 (chromates ions) and 4.9 (phosphates ions), and $\frac{1}{n}$ at 0.24 (chromates ions) and 0.20 (phosphates ions). To predict whether sorption under certain conditions is favorable, the partition coefficient R_L can be calculated for each measuring point. R_L is characteristic of systems described by the Langmuir isotherm. When the R_L is between 0–1, then adsorption on selected components is favorable. If $R_L > 1$, it means that the system has unfavorable sorption characteristics for the phenomenon studied. The relationship is calculated based on the following equations:

$$R_L = \frac{1}{1 + a_L C_0} \tag{2}$$

$$a_L = \frac{K_L}{q_{max}} \tag{3}$$

where:

R_L—partition coefficient;
a_L—the quotient of the equilibrium constant for the isotherm and the maximum area coverage for the model.

For the analyzed adsorption system, a graph of $R_L = f(C_0)$ was prepared (Figure 8). It shows that the calculated parameter is in the range from 0 to 1. This means that the surface phenomenon related to the removal of the examined ions is favorable.

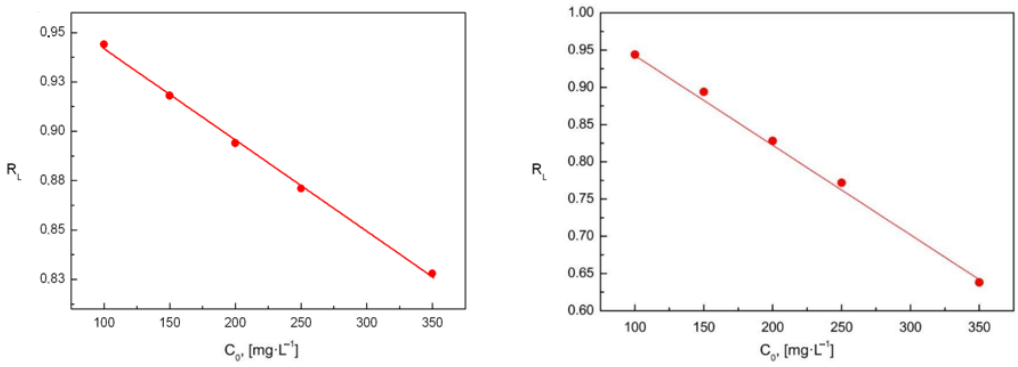

(**a**) (**b**)

Figure 8. Dependence of the equilibrium parameter R_L on the initial concentration of: (**a**) chromates ions and (**b**) phosphates ions in aqueous solutions for the Langmuir isotherm.

The Langmuir maximal adsorption capacity of Absodan Plus converted to phosphorus is 9.46 mg P/g. It is rather a high capacity compared to other capacities obtained for natural diatomites and ranges from 0.46–3.51 mg P/g (Table 7). The Absodan Plus adsorption capacity converted to chrome is 39.1 mg Cr/g. It is a very good result compared to capacities of calcined diatomite and raw Carpathian diatomite equal to 0.2 mg Cr/g and 0.12 mg Cr/g respectively [48,49]. As shown in Table 8, the adsorption capacity of Absodan Plus is satisfactory compared to unmodified diatomites. Various modifications lead to an increase in the efficiency of removing of phosphates and chromates by the transformed surface of the diatomite. A much higher removal capacity can be achieved by lanthanum oxide modified diatomite [77] or MCM-41 composite with refined diatomite containing a higher concentration of diatom frustules [50]. However, they are more advanced materials that require special reagents to produce. It is also a mineral that effectively adsorbs phosphates by surface complexation and precipitation [78–80]. As shown in Table 8 diatomite coated by hydrous iron oxide and metallic iron/iron oxides are characterized by a significant increase in the adsorption capacity of phosphates and chromates [27,28]. Other studies have shown that hematite can adsorb chromates, especially in an acidic environment [81]. As shown by the XRD analysis, Absodan Plus contains an admixture of hematite, which can support the removal of chromium and phosphorus.

Table 8. The comparison of the adsorption capacity of Absodan Plus with capacities of various diatomaceous sorbents.

	Material	Maximal Adsorption Capacity, mg/g	Ref.
P	diatomite	0.46 mg P/g	[37]
	diatomite	0.60 mg P/g	[28]
	diatomite	3.51 mg P/g	[27]
	hydrous Fe oxide modified diatomite	5–25 mg P/g	[28]
	diatomite coated by Fe^0 and Fe oxides	37.0 mg P/g	[27]
	La oxide modified diatomite	58.7 mg P/g	[77]
	Absodan Plus	9.46 mg P/g	present study
Cr	calcined diatomite	0.20 mg Cr/g	[47]
	diatomite	0.12 mg Cr/g	[75]
	Fe oxide modified diatomite	6.10 mg Cr/g	[47]
	diatomite-MCM-41 composite	70.9 mg Cr/g	[50]
	Absodan Plus	39.1 mg Cr/g	present study

3.3. The Adsorption Kinetics

When the adsorbent surface is saturated with molecules of the adsorbed substance, the adsorption capacity deteriorates, and the process should be stopped. Changes in phosphate ions concentration in solution and on the surface of the adsorbent during the adsorption process are shown in Figure 9. During the adsorption process, there is an exponential increase in the concentration of phosphate ions immobilized on the surface of the Absodan Plus and a decrease in their concentration in the solution. The concentration of the tested ions on the adsorbent surface initially increases rapidly, and after about 2 h, it practically does not change. Initially, the decrease in the concentration of phosphate ions is significant, then it is slowed down to a constant value after about 2.5 h. The situation is similar in the case of chromate ions (Figure 9). The obtained results indicate that chromate ions had easier access to the active centers of diatomite, which was confirmed by the size of the analyzed ions (phosphate ions are higher than chromate ions).

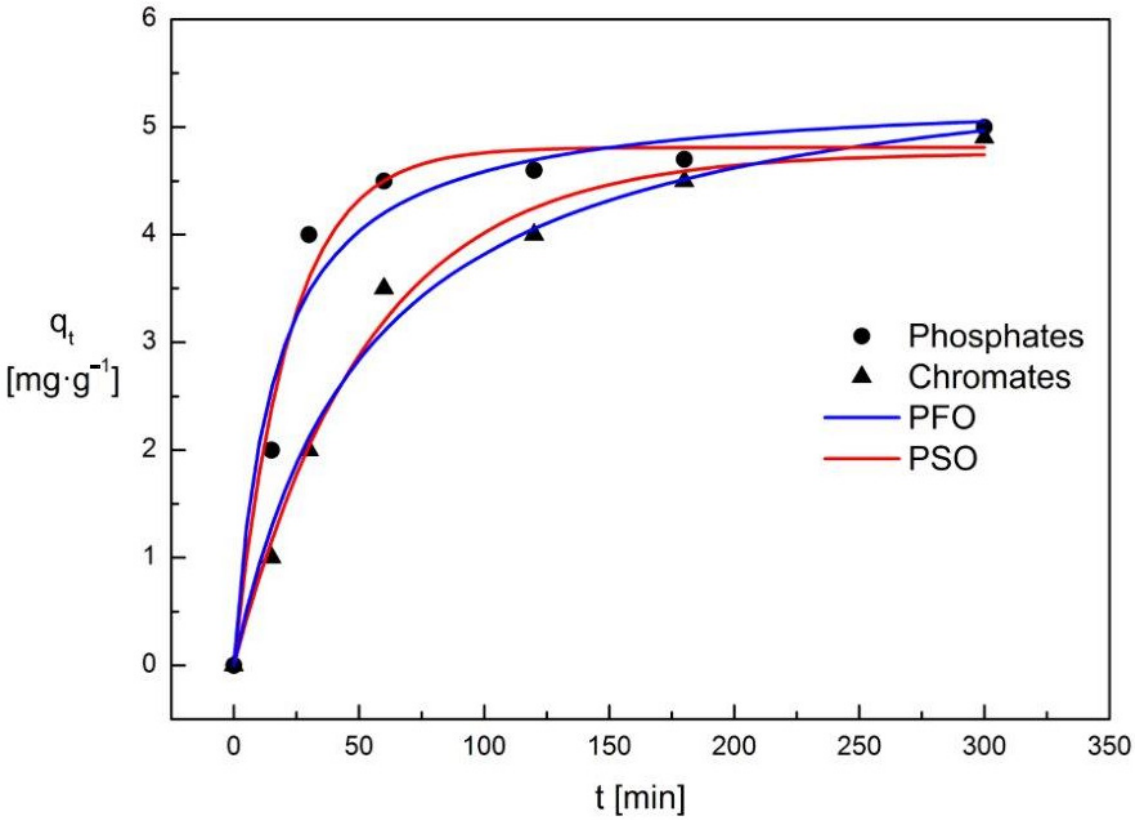

Figure 9. The pseudo-first-order and pseudo-second-order kinetic curves for the adsorption process for chromates and phosphates ions on an Absodan Plus.

To investigate the mechanism and determine the rate of the adsorption process, pseudo-first-order (PFO) and pseudo-second-order (PSO) kinetic models were developed (Table 9). Both the adsorbent and the adsorbate molecules could participate in the adsorption of chromates and phosphates ions on the diatomite. The analysis of pseudo kinetic curves showed that they were not linear (the kinetic equation is not fulfilled). The pseudo-second-order kinetic curves showed linear dependencies that go through the origin of the coordinate system (Figure 9). The pseudo-second-order kinetic equation has been met, as evidenced by a very good fit to the experimental data (R^2 values equal to 1). Three factors influence adsorption: the adsorbent, water, and the ions dissolved in it.

Table 9. Kinetic PSO and PFO model constants and correlation coefficients for the sorption systems.

Parameter	Pseudo-First-Order (PFO)		Pseudo-Second-Order (PSO)	
	Phosphates Ions	Chromates Ions	Phosphates Ions	Chromates Ions
χ^2/DoF	0.26	0.18	0.06	0.02
R^2	0.953	0.979	0.989	0.993
k_1 [min^{-1}]	$1.3 \cdot 10^{-2}$	$2.8 \cdot 10^{-3}$	$4.8 \cdot 10^{-2}$	$2.1 \cdot 10^{-2}$
q_e [mg·g^{-1}]	5.5	5.7	4.2	4.9

To determine the rate-limiting stage of the adsorption process, the intraparticle diffusion model developed by Weber and Morris [63] was used (Figure 10). The adsorption process can be divided into two stages: surface diffusion and intraparticle diffusion (mass transport takes place in each stage). The surface diffusion that occurs through the boundary layer is characterized by a high rate. Then the substance migrates deep into the structure of the diatomite, slowly filling the available pores until it fills their entire volume. The Weber model allows us to determine which of these stages affects the overall rate of adsorption [63].

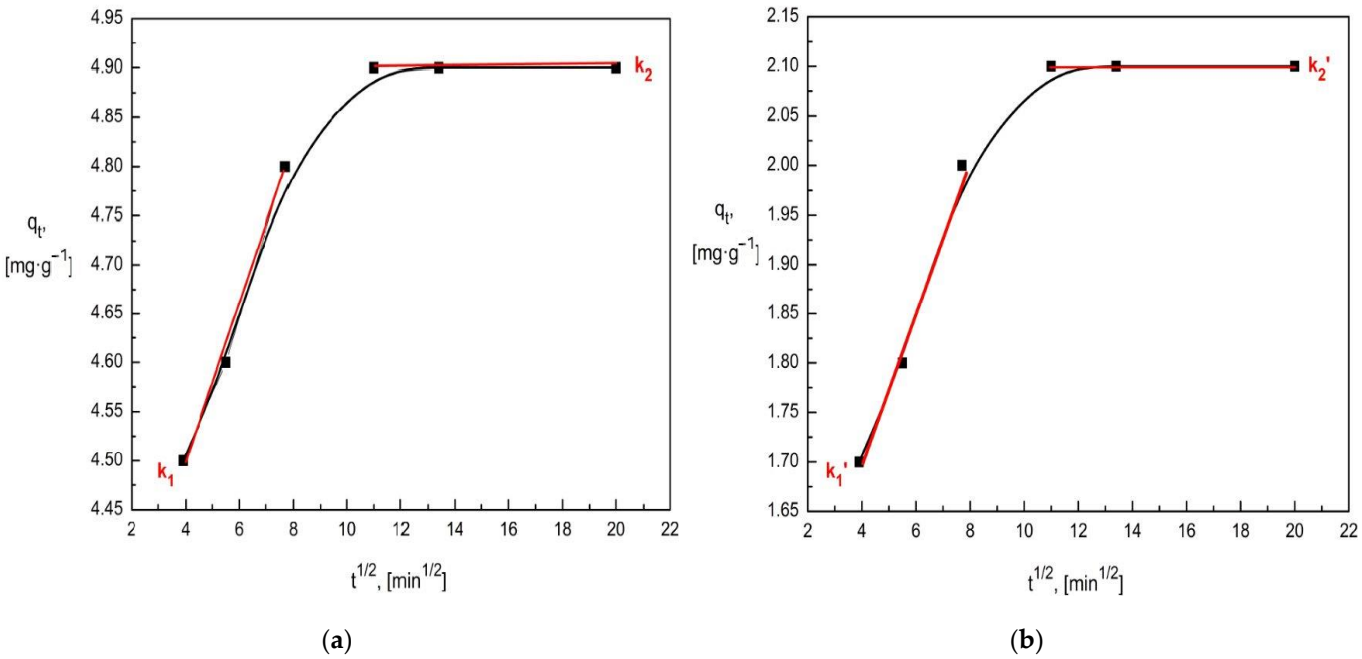

Figure 10. Intraparticle diffusion model in the diatomite adsorption process: (**a**) chromates ions, (**b**) phosphates ions.

The non-linear course of the entire adsorption process confirms that it is multistage. For the linear fragments in the diagrams (Figure 10), additional graphs were prepared and simple equations were determined. The slope values in the equations are equal to the diffusion process rate constant (Table 10). The first segment in the graphs is assigned to boundary layer diffusion, which is the main rate-limiting step for the entire process. The higher the value of the intercept in the equation of these lines, the greater the effect of boundary layer diffusion on the overall rate of the adsorption process. The second segment shows intraparticle diffusion. The slope values in the simple equations fitted to this stage correspond to the intraparticle diffusion constant (k_1, k_2), which in both cases is close and almost equal to zero. This is because this adsorption step is almost a constant function and does not significantly affect the rate of the entire process.

Table 10. Values of the diffusion rate constants of the phosphates and chromates adsorption process.

The Type of the Process	Line Equation	The Value of the Diffusion Rate Constant [mg/g·min$^{1/2}$]
Boundary layer diffusion for chromates ions	$q_t = 8{\cdot}10^{-2}{\cdot}t^{\frac{1}{2}} + 4.2$	$k_1 = 8{\cdot}10^{-2}$
Intraparticle diffusion for chromates ions	$q_t = 2.7{\cdot}10^{-15}{\cdot}t^{\frac{1}{2}} + 4.9$	$k_2 = 2.7{\cdot}10^{-15}$
Boundary layer diffusion for phosphates ions	$q_t = 8{\cdot}10^{-2}{\cdot}t^{\frac{1}{2}} + 1.4$	$k_1' = 8{\cdot}10^{-2}$
Intraparticle diffusion for phosphate ions	$q_t = 2.5{\cdot}10^{-15}{\cdot}t^{\frac{1}{2}} + 2.1$	$k_2' = 2.5{\cdot}10^{-15}$

4. Conclusions

The Absodan Plus is a diatomite commercial material containing an amorphous phase (33%) and also the crystalline phase of quartz, hematite, and grossite. The material is macro and mesoporous and its specific surface area is about 30 m^2/g. Its PZC is around pH = 5.5–6.0 and in an acidic environment is able to adsorb the anions. The saturation of the adsorbent surface with the adsorbed anions occurs after 2 h for chromates ions and 2.5 h for phosphates ions. The results obtained indicate that chromate ions had easier access to the diatomite's activity centers. Among the analyzed models of isotherms, the Redlich-Peterson isotherm is the best fit for the experimental points (R_2 = 0.975 and 0.994 for chromates and phosphates ions, respectively) showed. The rate-limiting stage of the adsorption of chromates and phosphates ions on diatomite is diffusion in the boundary layer. Intraparticle diffusion slightly affects the kinetics of the process. The maximum adsorption capacity of Absodan Plus in terms of phosphorus and chromium amounts to 9.46 mg P/g and 39.1 mg Cr/g, respectively. The adsorption capacity of Absodan Plus is satisfactory compared to unmodified diatomites. Various modifications lead to an increase in the phosphate and chromate removal efficiency by the reshaped diatomaceous earth surface. As shown by XRD analysis, Absodan Plus contains an admixture of hematite, which can support the removal of chromium and phosphorus.

Author Contributions: Conceptualization, E.S., M.M.M., D.P. (Dorota Papciak) and A.D.; methodology, E.S., B.C. and D.P. (Dariusz Pająk); software, B.C. and D.P. (Dariusz Pająk); formal analysis, E.S., M.M.M. and D.P. (Dorota Papciak); investigation, E.S., B.C. and D.P. (Dariusz Pająk); resources, E.S.; writing—original draft preparation, E.S., D.P. (Dorota Papciak) and A.D.; writing—review and editing, M.M.M. and B.C.; visualization, E.S., M.M.M. and A.D.; supervision, E.S. and M.M.M.; project administration, E.S.; funding acquisition, E.S., D.P. (Dorota Papciak) and M.M.M. All authors have read and agreed to the published version of the manuscript.

Funding: This research was funded under the UPB contract: PB29.B0.22.001.

Institutional Review Board Statement: Not applicable.

Informed Consent Statement: Not applicable.

Data Availability Statement: Not applicable.

Conflicts of Interest: The authors declare no conflict of interest.

References

1. Kazakis, N.; Kantiranis, N.; Kalaitzidou, K.; Kaprara, E.; Mitrakas, M.; Frei, R.; Vargemezis, G.; Tsourlos, P.; Zouboulis, A.; Filippidis, A. Origin of hexavalent chromium in groundwater: The example of Sarigkiol Basin, Northern Greece. *Sci. Total Environ.* **2017**, *593–594*, 552–566. [CrossRef] [PubMed]
2. Boujelben, R.; Ellouze, M.; Aziz, F.; Ouazzani, N.; Sayadi, S. Box-Behnken approach for optimization of Cr(III) removal from a real tanning effluent using powdered marble. *Int. J. Environ. Sci. Technol.* **2022**, *19*, 4305–4320. [CrossRef]
3. Tumolo, M.; Ancona, V.; De Paola, D.; Losacco, D.; Campanale, C.; Massarelli, C.; Uricchio, V.F. Chromium Pollution in European Water, Sources, Health Risk, and Remediation Strategies: An Overview. *Int. J. Environ. Res. Public Health* **2020**, *17*, 5438. [CrossRef] [PubMed]

4. Chen, S.-S.; Cheng, C.-Y.; Li, C.-W.; Chai, P.-H.; Chang, Y.-M. Reduction of chromate from electroplating wastewater from pH 1 to 2 using fluidized zero valent iron process. *J. Hazard. Mater.* **2007**, *142*, 362–367. [CrossRef] [PubMed]
5. Castro, L.; Rocha, F.; Muñoz, J.Á.; González, F.; Blázquez, M.L. Batch and Continuous Chromate and Zinc Sorption from Electroplating Effluents Using Biogenic Iron Precipitates. *Minerals* **2021**, *11*, 349. [CrossRef]
6. Chowdhury, M.; Mostafa, M.G.; Biswas, T.K.; Mandal, A.; Saha, A.K. Characterization of the Effluents from Leather Processing Industries. *Environ. Process.* **2015**, *2*, 173–187. [CrossRef]
7. Genawi, N.M.; Ibrahim, M.H.; El-Naas, M.H.; Alshaik, A.E. Chromium Removal from Tannery Wastewater by Electrocoagulation: Optimization and Sludge Characterization. *Water* **2020**, *12*, 1374. [CrossRef]
8. Mamun, A.A.; Khin, M.M.; Granata, G.; Tokoro, C. Removal of chromate from tannery wastewater: The applicability of sulfate-green rust in real coprecipitation processes. *Resour. Process.* **2018**, *65*, 67–73. [CrossRef]
9. Dresel, P.E.; Qafoku, N.; McKinley, J.P.; Fruchter, J.S.; Ainsworth, C.C.; Liu, C.; Ilton, E.S.; Phillips, J.L. *Geochemical Characterization of Chromate Contamination in the 100 Area Vadose Zone at the Hanford Site*; Pacific Northwest National Lab. (PNNL): Richland, WA, USA, 2008.
10. Wanner, C.; Eggenberger, U.; Kurz, D.; Zink, S.; Mäder, U. A chromate-contaminated site in southern Switzerland—Part 1: Site characterization and the use of Cr isotopes to delineate fate and transport. *Appl. Geochem.* **2012**, *27*, 644–654. [CrossRef]
11. Ulén, B.; Bechmann, M.; Fölster, J.; Jarvie, H.P.; Tunney, H. Agriculture as a phosphorus source for eutrophication in the north-west European countries, Norway, Sweden, United Kingdom and Ireland: A review. *Soil Use Manag.* **2007**, *23*, 5–15. [CrossRef]
12. Nortjé, G.P.; Laker, M.C. Factors That Determine the Sorption of Mineral Elements in Soils and Their Impact on Soil and Water Pollution. *Minerals* **2021**, *11*, 821. [CrossRef]
13. *Source Apportionment of Nitrogen and Phosphorus Inputs into the Aquatic Environment*; European Environment Agency Report No 7/2005; Office for Official Publications of the European Communities: Luxembourg, 2005.
14. Bunce, J.T.; Ndam, E.; Ofiteru, I.D.; Moore, A.; Graham, D.W. A Review of Phosphorus Removal Technologies and Their Applicability to Small-Scale Domestic Wastewater Treatment Systems. *Front. Environ. Sci.* **2018**, *6*, 8. [CrossRef]
15. Andreo-Martínez, P.; García-Martínez, N.; Almela, L. Domestic Wastewater Depuration Using a Horizontal Subsurface Flow Constructed Wetland and Theoretical Surface Optimization: A Case Study under Dry Mediterranean Climate. *Water* **2016**, *8*, 434. [CrossRef]
16. Kuo, Y.-M.; Muñoz-Carpena, R. Simplified modeling of phosphorus removal by vegetative filter strips to control runoff pollution from phosphate mining areas. *J. Hydrol.* **2009**, *378*, 343–354. [CrossRef]
17. Villalba, G.; Liu, Y.; Schroder, H.; Ayres, R.U. Global Phosphorus Flows in the Industrial Economy From a Production Perspective. *J. Ind. Ecol.* **2008**, *12*, 557–569. [CrossRef]
18. Grzmil, B.; Wronkowski, J. Removal of phosphates and fluorides from industrial wastewater. *Desalination* **2006**, *189*, 261–268. [CrossRef]
19. Khaled, B.; Wided, B.; Béchir, H.; Elimame, E.; Mouna, L.; Zied, T. Investigation of electrocoagulation reactor design parameters effect on the removal of cadmium from synthetic and phosphate industrial wastewater. *Arab. J. Chem.* **2019**, *12*, 1848–1859. [CrossRef]
20. Karn, R.; Ojha, N.; Abbas, S.; Bhugra, S. A review on heavy metal contamination at mining sites and remedial techniques. *IOP Conf. Ser. Earth Environ. Sci.* **2021**, *796*, 012013. [CrossRef]
21. Li, T.; Dong, W.; Zhang, Q.; Xing, D.; Ai, W.; Liu, T. Phosphate removal from industrial wastewater through in-situ Fe^{2+} oxidation induced homogenous precipitation: Different oxidation approaches at wide-ranged pH. *J. Envir. Manag.* **2020**, *255*, 109849. [CrossRef]
22. Minas, F.; Chandravanshi, B.S.; Leta, S. Chemical Precipitation Method For Chromium Removal And Its Recovery From Tannery Wastewater In Ethiopia. *Chem. Int.* **2017**, *3*, 291–305.
23. Omor, A.; Oubenali, A.A.; Oulbacha, M.; Majbar, Z.; Indrissi, N.; Elmadani, F.Z.; Metarfi, Y.; Ben Abbou, M.; Rais, Z. Environmental risk analysis of a dechromating station of chromate waste water. *J. Appl. Sci. Environ. Stud.* **2018**, *1*, 74–82.
24. Peng, H.; Leng, Y.; Cheng, Q.; Shang, Q.; Shu, J.; Guo, J. Efficient Removal of Hexavalent Chromium from Wastewater with Electro-Reduction. *Processes* **2019**, *7*, 41. [CrossRef]
25. Plummer, S.; Gorman, C.; Henrie, T.; Shimabuku, K.; Thompson, R.; Seidel, C. Optimization of strong-base anion exchange O&M costs for hexavalent chromium treatment. *Water Res.* **2018**, *139*, 420–433. [PubMed]
26. Kan, C.-C.; Ibe, A.H.; Rivera, K.K.P.; Arazo, R.O.; de Luna, M.D.G. Hexavalent chromium removal from aqueous solution by adsorbents synthesized from groundwater treatment residuals. *Sustain. Environ. Res.* **2017**, *27*, 163–171. [CrossRef]
27. Wang, J.; Zhang, G.; Qiao, S.; Zhou, J. Magnetic Fe^0/iron oxide-coated diatomite as a highly efficient adsorbent for recovering phosphorus from water. *Chem. Eng. J.* **2021**, *412*, 128696. [CrossRef]
28. Wang, Z.; Lin, Y.; Wu, D.; Kong, H. Hydrous iron oxide modified diatomite as an active filtration medium for phosphate capture. *Chemosphere* **2016**, *144*, 1290–1298. [CrossRef]
29. Alemayehu, E.; Thiele-Bruhn, S.; Lennartz, B. Adsorption behaviour of Cr (VI) onto macro and micro-vesicular volcanic rocks from water. *Sep. Purif. Technol.* **2011**, *78*, 55–61. [CrossRef]
30. Memedi, H.; Atkovska, K.; Lisichkov, K.; Marinkovski, M.; Kuvendziev, S.; Bozinovski, Z.; Reka, A.A. Removal of Cr (VI) From Water Resources by Using Different Raw Inorganic Sorbents. *Qual. Life* **2016**, *14*, 77–85. [CrossRef]

31. Zhang, B.; Wang, X.; Li, S.; Liu, Y.; An, Y.; Zheng, X. Preferable Adsorption of Nitrogen and Phosphorus from Agricultural Wastewater Using Thermally Modified Zeolite–Diatomite Composite Adsorbent. *Water* **2019**, *11*, 2053. [CrossRef]
32. Gubernat, S.; Masłoń, A.; Czarnota, J.; Koszelnik, P. Reactive Materials in the Removal of Phosphorus Compounds from Wastewater—A Review. *Materials* **2020**, *13*, 3377. [CrossRef]
33. Aljbour, S.H.; Al-Harahsheh, A.M.; Aliedeh, M.A.; Al-Zboon, K.; Al-Harahsheh, S. Phosphate removal from aqueous solutions by using natural Jordanian zeolitic tuff. *Adsorp. Sci. Technol.* **2017**, *35*, 284–299. [CrossRef]
34. Haldar, S.K.; Tišljar, J. *Introduction to Mineralogy and Petrology*; Elsevier: Amsterdam, The Netherlands, 2014.
35. Reka, A.A.; Pavlovski, B.; Fazlija, E.; Berisha, A.; Pacarizi, M.; Daghmehchi, M.; Sacalis, C.; Jovanovski, G.; Makreski, P.; Oral, A. Diatomaceous Earth: Characterization, thermal modification, and application. *Open Chem.* **2021**, *19*, 451–461. [CrossRef]
36. Figarska-Warchoł, B.; Stańczak, G.; Rembiś, M.; Toboła, T. Diatomaceous rocks of the Jawornik deposit (the Polish Outer Carpathians)-petrophysical and petrographical evaluatio. *Geol. Geophys. Environ.* **2015**, *41*, 311–331. [CrossRef]
37. Zahradník, J.; Jirásek, J.; Zahradník, J.; Sivek, M. Development of the diatomite production, reserves and its processing in the Czech Republic in 1999–2018. *Miner. Resour. Manag.* **2019**, *35*, 31–48.
38. Zhao, Y.; Tian, G.; Duan, X.; Liang, X.; Meng, J.; Liang, J. Environmental Applications of Diatomite Minerals in Removing Heavy Metals from Water. *Ind. Eng. Chem. Res.* **2019**, *58*, 11638–11652. [CrossRef]
39. Hernández-Ávila, J.; Salinas-Rodríguez, E.; Cerecedo-Sáenz, E.; Reyes-Valderrama, M.; Arenas-Flores, A.; Román-Gutiérrez, A.; Rodríguez-Lugo, V. Diatoms and Their Capability for Heavy Metal Removal by Cationic Exchange. *Metals* **2017**, *7*, 169. [CrossRef]
40. Benkacem, T.; Hamdi, B.; Chamayou, A.; Balard, H.; Calvet, R. Physicochemical characterization of a diatomaceous upon an acid treatment: A focus on surface properties by inverse gas chromatography. *Powder Technol.* **2016**, *294*, 498–507. [CrossRef]
41. Bandura, L.; Woszuk, A.; Kołodyńska, D.; Franus, W. Application of Mineral Sorbents for Removal of Petroleum Substances: A Review. *Minerals* **2017**, *7*, 37. [CrossRef]
42. Kaleta, J.; Papciak, D.; Puszkarewicz, A. Klinoptylolity i diatomity w aspekcie przydatności w uzdatnianiu wody i oczyszczaniu ścieków. *Gospod. Surowcami Miner.* **2007**, *23*, 21–34. (In Polish)
43. Zamorska, J.; Papciak, D. Activity of nitrifying biofilm in the process of water treatment in diatomite bed. *Environ. Prot. Eng.* **2008**, *34*, 37–52.
44. Yuan, P.; Wu, D.Q.; He, H.P.; Lin, Z.Y. The hydroxyl species and acid sites on diatomite surface: A combined IR and Raman study. *Appl. Surf. Sci.* **2004**, *227*, 30–39. [CrossRef]
45. Bello, O.S.; Adegoke, K.A.; Oyewole, R.O. Insights into the Adsorption of Heavy Metals from Wastewater using Diatomaceous Earth. *Sep. Sci. Technol.* **2014**, *49*, 1787–1806. [CrossRef]
46. Danil de Namor, A.F.; El Gamouz, A.; Frangie, S.; Martinez, V.; Valiente, L.; Webb, O.A. Turning the volume down on heavy metals using tuned diatomite. A review of diatomite and modified diatomite for the extraction of heavy metals from water. *J. Hazard. Mater.* **2012**, *241–242*, 14–31. [CrossRef] [PubMed]
47. Zhang, J.; Ding, T.; Zhang, Z.; Xu, L.; Zhang, C. Enhanced Adsorption of Trivalent Arsenic from Water by Functionalized Diatom Silica Shells ed W-C Chin. *PLoS ONE* **2015**, *10*, e0123395. [CrossRef]
48. Puszkarewicz, A.; Kaleta, J. Adsorption of Chromium (VI) on Raw and Modified Carpathian Diatomite. *J. Ecol. Eng.* **2019**, *20*, 11–17. [CrossRef]
49. Sungworawongpana, S.; Pengprecha, S. Calcination Effect of Diatomite to Chromate Adsorption. *Procedia Eng.* **2011**, *8*, 53–57. [CrossRef]
50. Selim, A.Q.; Mohamed, E.A.; Mobarak, M.; Zayed, A.M.; Seliem, M.K.; Komarneni, S. Cr (VI) uptake by a composite of processed diatomite with MCM-41: Isotherm, kinetic and thermodynamic studies. *Microporous Mesoporous Mater.* **2018**, *260*, 84–92. [CrossRef]
51. An Investigation of the Sorption of Arsenic by Diatomite (WC/99/020). Available online: https://www.gov.uk/research-for-development-outputs/an-investigation-of-the-sorption-of-arsenic-by-diatomite-wc-99-020 (accessed on 12 March 2022).
52. Eynard, U.; Georgitzikis, K.; Wittmer, D.; Latunussa, C.E.L.; Torres de Matos, C.; Mancini, L.; Unguru, M.; Blagoeva, D.; Bobba, S.; Pavel, C.; et al. *2020 European Commission, Study on the EU's List of Critical Raw Materials (2020)—Final Report (2020)*; Publications Office of the European Union: Luxembourg, 2020.
53. Commercial Data of Granular Diatomite DETM. Available online: https://epminerals.com/products/oil-absorbent-de (accessed on 12 March 2022).
54. Commercial Data of Granular Diatomite Damolex, C. Available online: https://mistralni.co.uk/products/diatomaceous-earth-granular-diatomite-damolex-c-1-3mm (accessed on 12 March 2022).
55. Commercial Data of Granular Diatomite Absodan Plus. Available online: https://www.damolin.com.pl/pl/p/Sorbent-ABSODAN-Plus-DAMOLIN-worek-10-Kg/175 (accessed on 12 March 2022).
56. ElSayed, E.E. Natural diatomite as an effective adsorbent for heavy metals in water and wastewater treatment (a batch study). *Water Sci.* **2018**, *32*, 32–43. [CrossRef]
57. Datta, J. Stiffness and energy dissipation of poly(etherurethane) resilient elements. *Chem. Rev.* **2015**, *1*, 116–119. (In Polish) [CrossRef]
58. Sočo, E.; Papciak, D.; Michel, M.M.; Pająk, D.; Domoń, A.; Kupiec, B. Characterization of the Physical, Chemical, and Adsorption Properties of Coal-Fly-Ash–Hydroxyapatite Composites. *Minerals* **2021**, *11*, 774. [CrossRef]

59. Markmanuel, D.; Tarawou, T.; Horsfall, M. Determination of Sodium Sorption Capacity Using the Boehm Metho Research. *J. Chem. Sci.* **2013**, *3*, 1–4.
60. Pretoriusa, P.J.; Woolardb, C.D. The Surface Chemical Properties of Novel High Surface Area Solids Synthesized from Coal Fly Ash. *S. Afr. J. Chem.* **2003**, *56*, 34–39.
61. Fiol, N.; Villaescusa, I. Determination of sorbent point zero charge: Usefulness in sorption studies. *Environ. Chem. Lett.* **2009**, *7*, 79–84. [CrossRef]
62. Al-Ghouti, M.A.; Da'ana, D.A. Guidelines for the use and interpretation of adsorption isotherm models: A review. *J. Hazard. Mater.* **2020**, *393*, 122383. [CrossRef] [PubMed]
63. Weber, W.J.J.; Morris, J.C. Kinetics of adsorption on carbon from solution. *J. Sanit. Eng. Div.* **1963**, *89*, 31–59. [CrossRef]
64. Freundlich, H.M.F. Over the Adsorption in Solution. *J. Phys. Chem.* **1906**, *57*, 385–471.
65. Liu, X.; Zhang, L. Removal of phosphate anions using the modified chitosan beads: Adsorption kinetic, isotherm and mechanism studies. *Powder Technol.* **2015**, *277*, 112–119. [CrossRef]
66. Langmuir, I. The constitution and fundamental properties of solids and liquids. Part I. solids. *J. Am. Chem. Soc.* **1916**, *38*, 2221–2295. [CrossRef]
67. Qu, B.; Zhou, J.; Xiang, X.; Zheng, C.; Zhao, H.; Zhou, X. Adsorption behavior of Azo Dye C. I. Acid Red 14 in aqueous solution on surface soils. *J. Environ. Sci.* **2008**, *20*, 704–709. [CrossRef]
68. Jovanovich, D.S. Physical adsorption of gases I: Isotherms for monolayer and multilayer adsorption. *Colloid Polym. Sci.* **1969**, *235*, 1203–1214.
69. Halsey, G.D. The Role of Surface Heterogeneity in Adsorption. *Adv. Catal.* **1952**, *4*, 259–269.
70. Gholitabar, S.; Tahermansouri, H. Kinetic and multi-parameter isotherm studies of picric acid removal from aqueous solutions by carboxylated multi-walled carbon nanotubes in the presence and absence of ultrasound. *Carbon Lett.* **2017**, *22*, 14–24.
71. Reczek, L.; Michel, M.M.; Trach, Y.; Siwiec, T.; Tytkowska-Owerko, M. The Kinetics of Manganese Sorption on Ukrainian Tuff and Basalt—Order and Diffusion Models Analysis. *Minerals* **2020**, *10*, 1065. [CrossRef]
72. Mozgawa, W.; Król, M.; Bajda, T. Application of IR spectra in the studies of heavy metal cations immobilization on natural sorbents. *J. Mol. Struct.* **2009**, *924–926*, 427–433. [CrossRef]
73. Almasri, D.A.; Saleh, N.B.; Atieh, M.A.; McKay, G.; Ahzi, S. Adsorption of phosphate on iron oxide doped halloysite nanotubes. *Sci. Rep.* **2019**, *9*, 3232. [CrossRef]
74. Shabalala, A.N.; Basitere, M. Interactive Relationship between Cementitious Materials and Acid Mine Drainage: Their Effects on Chromium Cr(VI) Removal. *Minerals* **2020**, *10*, 932. [CrossRef]
75. Mishima, K.; Du, X.; Sekiguchi, S.; Kano, N. Experimental and Theoretical Studies on the Adsorption and Desorption Mechanisms of Chromate Ions on Cross-Linked Chitosan. *J. Funct. Biomater.* **2017**, *8*, 51. [CrossRef]
76. Ojediran, J.O.; Dada, A.O.; Aniyi, S.O.; David, R.O.; Adewumi, A.D. Mechanism and isotherm modeling of effective adsorption of malachite green as endocrine disruptive dye using Acid Functionalized Maize Cob (AFMC). *Sci. Rep.* **2021**, *11*, 21498. [CrossRef]
77. Wu, Y.; Li, X.; Yang, Q.; Wang, D.; Xu, Q.; Yao, F.; Chen, F.; Tao, Z.; Huang, X. Hydrated lanthanum oxide-modified diatomite as highly efficient adsorbent for low-concentration phosphate removal from secondary effluents. *J. Environ. Manag.* **2019**, *231*, 370–379. [CrossRef]
78. Liu, J.; Zhu, R.; Ma, L.; Fu, H.; Lin, X.; Parker, S.C.; Molinari, M. Adsorption of phosphate and cadmium on iron (oxyhydr)oxides: A comparative study on ferrihydrite, goethite, and hematite. *Geoderma* **2021**, *383*, 114799. [CrossRef]
79. Elzinga, E.J.; Sparks, D.L. Phosphate adsorption onto hematite: An in situ ATR-FTIR investigation of the effects of pH and loading level on the mode of phosphate surface complexation. *J. Colloid Interface Sci.* **2007**, *308*, 53–70. [CrossRef]
80. Wang, L.; Putnis, C.; Hövelmann, J.; Putnis, A. Interfacial Precipitation of Phosphate on Hematite and Goethite. *Minerals* **2018**, *8*, 207. [CrossRef]
81. Ajouyed, O.; Hurel, C.; Ammari, M.; Allal, L.B.; Marmier, N. Sorption of Cr(VI) onto natural iron and aluminum (oxy)hydroxides: Effects of pH, ionic strength and initial concentration. *J. Hazard. Mater.* **2010**, *174*, 616–622. [CrossRef]